Increased Alpha-Band Connectivity During Tic Suppression in Children With Tourette Syndrome Revealed by Source Electroencephalography Analyses

Supplement

Supplementary methods

Participants

Criteria for inclusion were (i) having motor and/or phonic tics on a regular basis for at least one year and (ii) ages between 8 and 16 years old. Criteria for exclusion were a history of (i) neurological illness, seizures, or head trauma with loss of consciousness, (ii) intellectual disability, (iii) autism spectrum disorder, and (iv) severe major depressive disorder, as assessed by the semi-structured interview.

All 72 participants had motor tics at the time of testing. Their YGTSS motor tics subscale score ranged from 7 to 21. Fourteen of the 72 participants had no phonic tic at the time of testing (YGTSS phonic tics subscale score of 0). The YGTSS phonic tic subscale score of the 58 participants with phonic tics ranged from 3 to 19.

While some children reported past or current psychotherapy or counseling, none had previously received habit reversal training (HRT) or Comprehensive Behavioral Intervention for Tics (CBIT).

Clinical assessment

Tic severity was assessed with the Yale Global Tic Severity Scale (YGTSS; 1), which was administered by licensed clinicians with expertise in TS. The YGTSS assesses motor and phonic tics on a 6-point scale (0-5) according to 5 dimensions of tics: number, frequency, intensity, complexity, and interference. Therefore, the YGTSS yields a score for motor and for phonic tic severity, which ranges from 0 to 25. These two scores are added up to form the total tic score, which ranges from 0 to 50. The latter score was used at the primary measure of tic severity in the current study.

ADHD symptoms were assessed with the 18-item version of Swanson, Nolan and Pelham Questionnaire (SNAP-IV; 2). Each item was scored by one of the child's parent, on a 4-point Likert scale (0-3). Therefore,

SNAP-IV scores range from 0 (no ADHD symptom at all) to 54 (most severe). Anxiety symptoms were assessed with the Screen for Child Anxiety Related Disorders (SCARED; 3), which is a 41-item parent-rated questionnaire. The SCARED is rated on a 3-point Likert scale and yields a score ranging from 0 to 82. Severity of disruptive behaviors was assessed with the Disruptive Behavior Rating Scale (DBRS; 4), which is an 8-item inventory corresponding to the DSM-IV-TR (5) criteria for oppositional defiant disorder (ODD). The DBRS is rated by parents on a 4-point Likert scale, where they indicate how frequently their child engaged in each type of behavior in the past 6 months. Severity of depression symptoms was assessed with the Anxious/Depressed and the Withdrawn/Depressed Scales of the Child Behavior Checklist (6). CBCL is one of the best-researched and most widely-used parent ratings of child psychopathology, has two factor-analytically derived scales of depressive symptoms inquiring about sad mood, feelings of worthless, lack of energy and anhedonia. Items are rated on a 3-point Likert scale and raw scores are converted to T-scores that are based on large standardization sample with a mean of 50, and standard deviation 10. Higher scores indicate greater severity.

Children's IQ was estimated using the Weschler Abbreviated Scale of Intelligence (WASI; 7). Handedness was assessed with the Edinburgh Handedness Inventory (8).

Experimental procedures

Children with TS were required to suppress their tics during three 2-minute sessions while keeping their eyes open. They were allow to take a short break between each session. Immediately following these tic suppression sessions, EEG was recorded during a 7-minute resting session when children were allowed to tic freely, also while keeping their eyes open.

In 10 children who performed an early version of this task, only 2 tic suppressions sessions were performed. One child performed a single 2-minute session of tic suppresion. Also, in 7 children, it was only possible to record 2 minutes of resting EEG. To ascertain that our results are not attributable to these slight variations in task duration, supplementary analyses were performed on children with three 2-minute tic suppression sessions and 7 minutes of rest (n = 50; see Supplementary Results).

EEG preprocessing

The first step of the Maryland Analysis of Developmental EEG (MADE) pipeline consists in offline filtering of the data using EEGLAB's firfilt plugin. Continuous data were filtered with a Hamming window finite impulse response (FIR) filter, with a 1 Hz high-pass filter (0.3 Hz transition width) and a 50 Hz low-pass filter (10 Hz transition width). The stopband attenuation was 53 dB. Movements during EEG recordings, especially in pediatric populations with movement disorders, can lead some electrodes to be flat or noisy. It is therefore important to identify and remove bad channels. To this end, we used the *channel_properties* function from EEGLAB's FASTER plugin (9), which identifies bad channels according to three-values: Hurst exponent, correlation with other channels, and channel variance. After removal of bad channels, we used an independent component analysis (ICA) method to remove non-neural artifacts such as blinks, saccades, and muscle artifacts, which can be especially prevalent in children with TS. Since ICA performs better on data filtered with higher high-pass filter, the ICA was performed on a copy of the recordings, which is high-pass filtered at 1 Hz and epoched into 1-second segments. At this stage, epochs with very low/high amplitude epochs (± 1000 μV) and excessive EMG activity (exceeding -30 and 100 dB between 20-40 Hz) were identified. Channels containing more than 20% of these epochs, suggesting bad channels missed by FASTER, were removed from the copied and the original datasets. These bad epochs were then removed from the copied dataset. Then, the ICA was performed on the copied dataset using EEGLAB's runica function and ICA weights were transferred to the original dataset.

To automatically identify artifacted ICA components, the MADE pipeline uses a modified version of EEGLAB's ADJUST plugin (10), which is adapted for pediatric recordings (11). These ICA components that were identified as artifacts were subtracted from the original dataset and the EEG signal was thus corrected without losing data segments. Continuous data from both the tic suppression and rest sessions were then epoched into 2-seconds segments, which were used for cortical connectivity analyses. To remove any residual artifact following ICA cleaning, a threshold rejection method was applied. For frontal electrodes near the eyes (1, 8, 14, 21, 25, 32), any epoch with voltage exceeding ±100 μV was removed. For other electrodes, epochs with more than 10% of electrodes exceeding that threshold were removed. For remaining epochs, individual channels were interpolated with a spherical spline procedure at the epoch

level if they exceeded that threshold. Channels that were removed using the FASTER plugin were then interpolated, also with a spherical spline procedure. Finally, electrodes were re-referenced to the average reference.

Source-based connectivity pipeline

Brain sources were reconstructed with the Brainstorm toolbox (12). Electrode positions were co-registered to the MNI-ICBM152 template using three reference points (nasion, left, and right preauricular points). Using OpenMEEG (13), we computed a head model with the symmetric boundary element method (BEM). The BEM generates a three-layered head model (scalp, outer skull, and inner skull). The diagonal of the noise covariance matrix, which was computed for both conditions for each participant, was used for source reconstruction.

Graph theory analyses

We used a combination of methods to compute graph theory metrics relating to tic suppression. In the first step, the resulting weighted connectivity matrices were thresholded. Given the arbitrary nature of choosing a threshold and following the methods used by prior studies (14, 15), a wide range of thresholds were used to extract graph theory metrics. Proportional thresholds were used to keep the same number of edges in both conditions. Based on the work from Xu *et al.* (15), we computed graph theory metrics over 41 intervals, thus keeping between 10% and 50% (1% increments) of the highest PLV values. Our choice of eight graph theory metrics related to global network topology (strength (S_p), clustering coefficient (C_p) characteristic path length (L_p), global efficiency (E_{glob}), local efficiency (E_{loc}), normalized clustering coefficient (γ), normalized characteristic path length (λ), and small-worldness (σ)) was based on previous work (16, 17).

Strength is defined as the sum of each node's connection weight. The strength of a network is the average strength of all nodes in that network. The clustering coefficient measures how a node tends to cluster with adjacent nodes to form triplets of nodes. Therefore, the mean clustering coefficient of a network reflects how individual nodes are clustered. The characteristic path length represents the average shortest path between two nodes and is a measure of network integration. Another measure of integration if the global efficiency, which can be thought as the inverse of the characteristic path length. Global efficiency is more

influenced by short paths between nodes, while the characteristic path length is more influenced by long paths. The local efficiency of a node quantifies the communication between its adjacent nodes when that node is removed from the network (18, 19).

A small-world network is a network where adjacent nodes tend to cluster together, while at the same time having short path length, i.e. requiring few edges to connect two nodes (20-22). To calculate small-worldness, 100 random networks were derived from the original connectivity matrix for each participant and each condition. Normalized clustering coefficient (γ) is computed as $\gamma = C_p / C_p^{rand}$ and normalized characteristic path length (λ) is computed as $\lambda = L_p / L_p^{rand}$, where C_p^{rand} and L_p^{rand} are the mean clustering coefficient and the mean characteristic path length computed from 100 random networks, respectively. Small-worldness is computed as $\sigma = \gamma / \lambda$. Small-world networks are defined as being more clustered than random networks ($\gamma > 1$), while having similar characteristic path length ($\lambda \approx 1$), therefore showing high segregation and integration (19).

Since graph theory metrics were computed over 41 thresholds, each metric can be plotted as a function of graph density (i.e. the percentage of connections remaining in the graph). To limit the number of comparisons that could arise from using 41 thresholds, we computed the area under the curve (AUCs) for each metric. These AUCs were used as dependent variables in analyses pertaining to global network topology and nodal properties.

In the second step, graph theory metrics were computed on the network identified by NBS. NBS yields a binary matrix where the edges involved in the network are scored as 1, while the other edges are scored as 0. We first computed the degree of that matrix, which was used to define the sizes of the nodes on Figures depicting the networks identified by NBS. Then, the binary matrix was applied as a mask on each of the individual matrices of children with TS. More specifically, each individual connectivity matrix was multiplied by the binary matrix (consisting of 0's and 1's). This procedure allowed to keep the weights of edges that were part of the network identified by NBS, while setting all other edges to 0. Graph theory metrics were then calculated on these weighted matrices. We used the same metrics as those computed on thresholded matrices described above.

Network-based statistics

First, NBS involves mass univariate testing of each connection (using the general linear model; GLM). Then, connections exceeding a given threshold ($t = 3.44$ (corresponding to $\alpha = .0005$)) are admitted to a set of supra-threshold connections. Subsequently, connected graph components are identified among these supra-threshold connections. Finally, a p-value corrected for family-wise error rate (FWER) is calculated for each connected graph component using permutation testing with 5000 permutations (23, 24).

Supplementary results

Table S1: Connections between nodes in the alpha-band subnetwork

Connection	*t*-statistic
L postcentral gyrus – L precuneus	4.29
R cuneus – L postcentral	4.18
L banks of the superior temporal sulcus – L lingual gyrus	3.97
L caudal middle frontal gyrus – L precentral gyrus	3.96
L parahippocampal gyrus – L precentral gyrus	3.94
L banks of the superior temporal sulcus – L inferior temporal gyrus	3.86
L caudal middle frontal gyrus – R lateral occipital cortex	3.84
R caudal anterior cingulate gyrus – L precuneus	3.81
L inferior parietal cortex – R superior frontal gyrus	3.80
L isthmus of the cingulate cortex – L posterior cingulate cortex	3.78
L caudal middle frontal gyrus – R superior parietal cortex	3.78
L isthmus of the cingulate cortex – R superior frontal gyrus	3.75
L banks of the superior temporal sulcus – R lingual gyrus	3.70
R inferior parietal cortex – R superior frontal gyrus	3.70
L lateral occipital cortex – R superior frontal gyrus	3.70
L precuneus – R superior frontal gyrus	3.67
L parahippocampal gyrus – L transverse temporal cortex	3.67
R caudal anterior cingulate cortex – L superior parietal cortex	3.64
L caudal anterior cingulate cortex – L superior parietal cortex	3.60
L pars triangularis – R superior parietal cortex	3.60
L pericalcarine cortex – R superior frontal gyrus	3.59
L postcentral gyrus – L superior parietal cortex	3.57
R caudal middle frontal gyrus – L precuneus	3.56
R middle temporal gyrus – R superior frontal gyrus	3.54
R superior frontal gyrus – R superior parietal cortex	3.52
L precentral gyrus – L precuneus	3.51
R pericalcarine cortex – R superior frontal gyrus	3.50
L inferior parietal cortex – L superior frontal gyrus	3.45
L banks of the superior temporal sulcus – R superior frontal gyrus	3.44

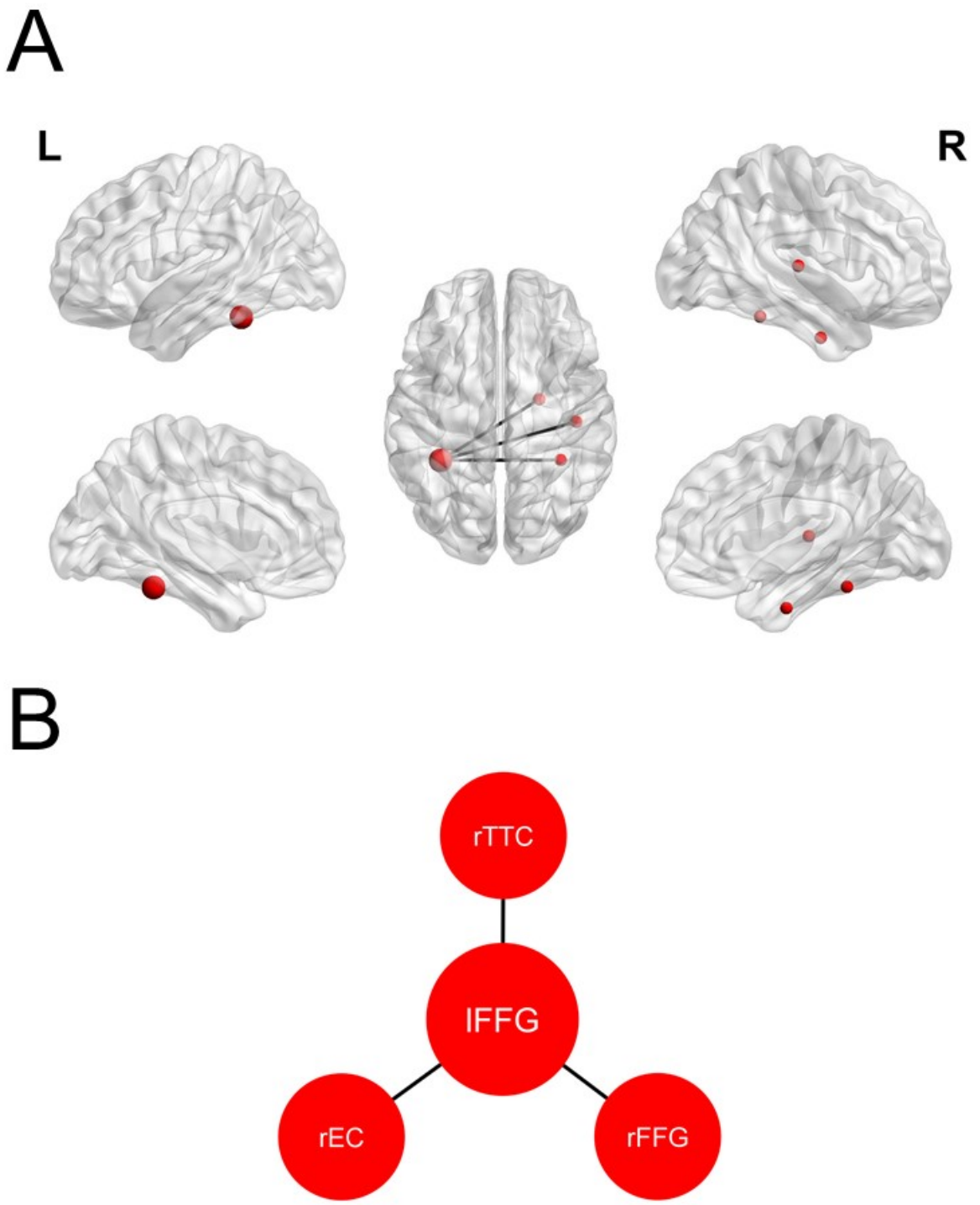

Figure S1: Second subnetwork of functional connectivity in the alpha band during tic suppression. (A) There was a second and smaller subnetwork that reach the significance threshold in the alpha band (p = .037, FWER-corrected). That subnetwork included 4 nodes and 3 edges. In this subnetwork, the left fusiform gyrus was connected to three other nodes. (B) graphical representation of the subnetwork. Note: "l" & "r" denotes the lateralization of the nodes; EC: entorhinal cortex, FFG: fusiform gyrus, TTC: transverse temporal cortex.

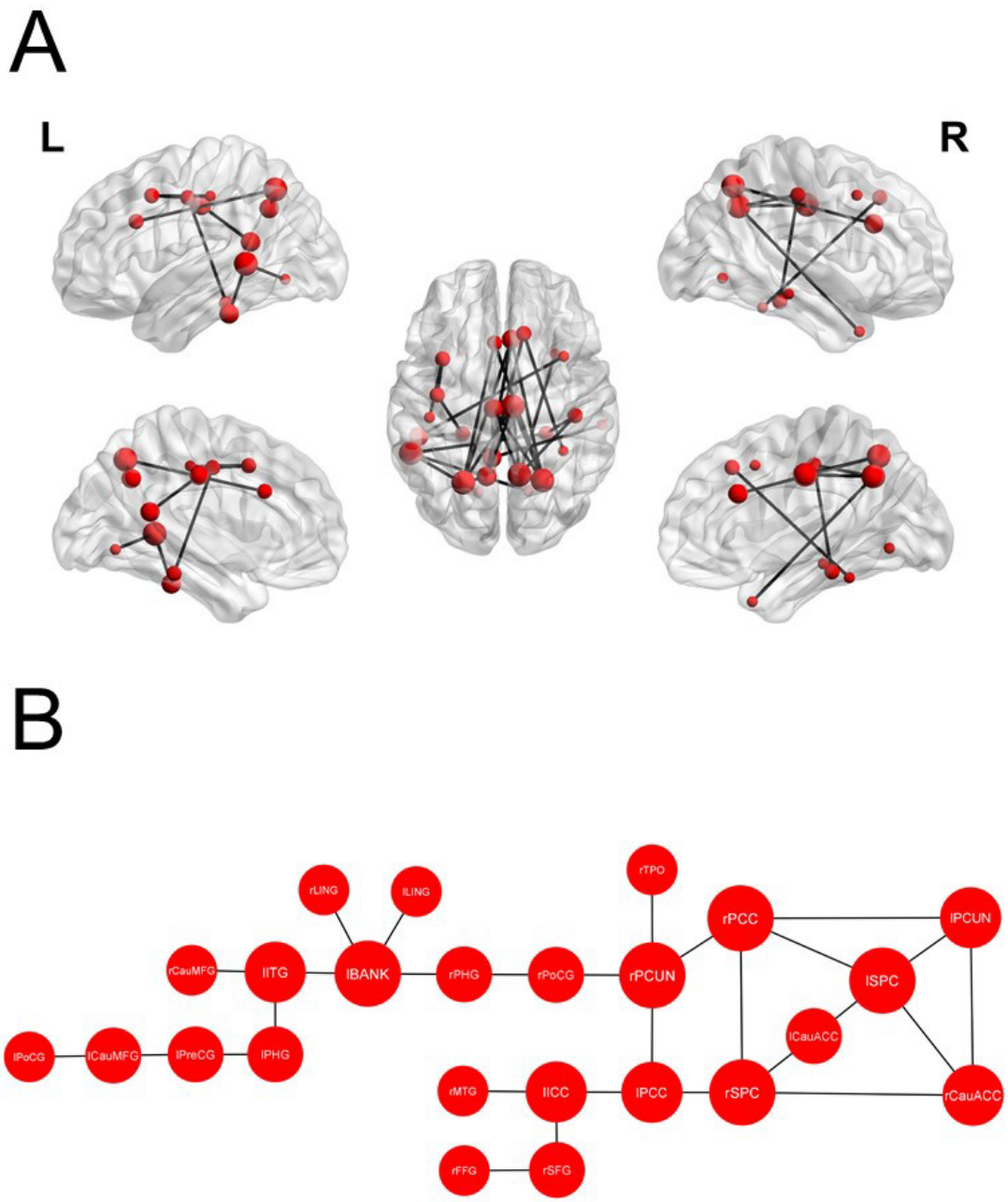

Figure S2: Subnetwork of functional connectivity in the theta band during tic suppression. (A) Compared to the rest condition, 24 nodes in this subnetwork showed increased connectivity during tic suppression ($p < .001$, FWER-corrected). Node size corresponds to connectivity degree (number of connections per node). In that subnetwork comprising 28 edges, 5 nodes had a connectivity degree of 4 and a degree z-score of 1.5: the left banks of the superior temporal sulcus, the right posterior cingulate cortex, the right precuneus, and the bilateral superior parietal cortex. (B) Graphical representation of the theta subnetwork. Note: "l" & "r" denotes the lateralization of the nodes; BANK: banks of the superior temporal sulcus, CauACC: caudal anterior cingulate cortex, CauMFG: caudal middle frontal gyrus, FFG: fusiform gyrus, ICC: isthmus of the cingulate cortex, ITG, inferior temporal gyrus, LING: lingual gyrus, MTG: middle temporal gyrus, PCC: posterior cingulate cortex, PCUN: precuneus, PHG: parahippocampal gyrus, PoCG: postcentral gyrus, PreCG: precentral gyrus, SFG: superior frontal gyrus, SPC: superior parietal cortex, TPO: temporal pole.

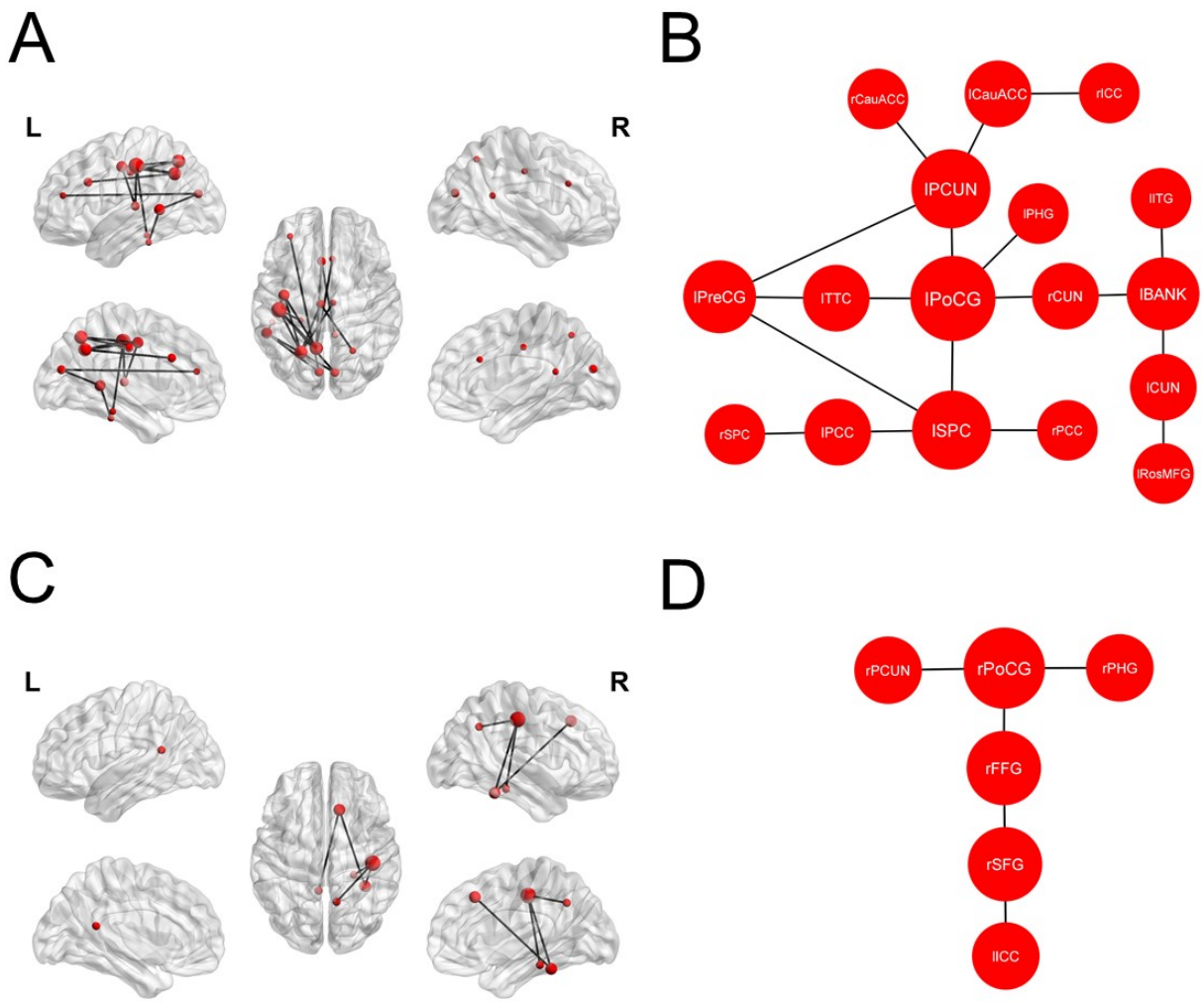

Figure S3: Subnetworks of functional connectivity in the beta band during tic suppression. NBS analyses revealed two subnetworks of increased functional connectivity in the beta band during tic suppression. Node size corresponds to connectivity degree (number of connections per node). (A) The first subnetwork comprised 17 nodes and 18 edges ($p < .001$, FWER-corrected). Here, the left postcentral gyrus (5 connections, degree z-score: 2.3), the left precuneus (4 connections, degree z-score: 1.5), and the left superior parietal cortex (4 connections, degree z-score: 1.5) were considered as hubs. (B) Graphical representation of the first beta subnetwork. (C) The second subnetwork only included 6 nodes and 5 edges ($p = .006$, FWER-corrected). In that subnetwork, the only hub was the right postcentral gyrus (degree z-score: 1.6) which was connected to three other nodes. (D) Graphical representation of the second beta subnetwork. Note: “l” & “r” denotes the lateralization of the nodes; BANK: bank of the superior temporal sulcus, CauACC: caudal anterior cingulate cortex, CUN: cuneus, FFG: fusiform gyrus, ICC: isthmus of the cingulate cortex, ITG: inferior temporal gyrus, PCC: posterior cingulate cortex, PCUN: precuneus, PHG: parahippocampal gyrus, PoCG: postcentral gyrus, PreCG: precentral gyrus, RosMFG: rostral middle frontal gyrus, SFG: superior frontal gyrus, SPC: superior parietal cortex, TTC: transverse temporal cortex.

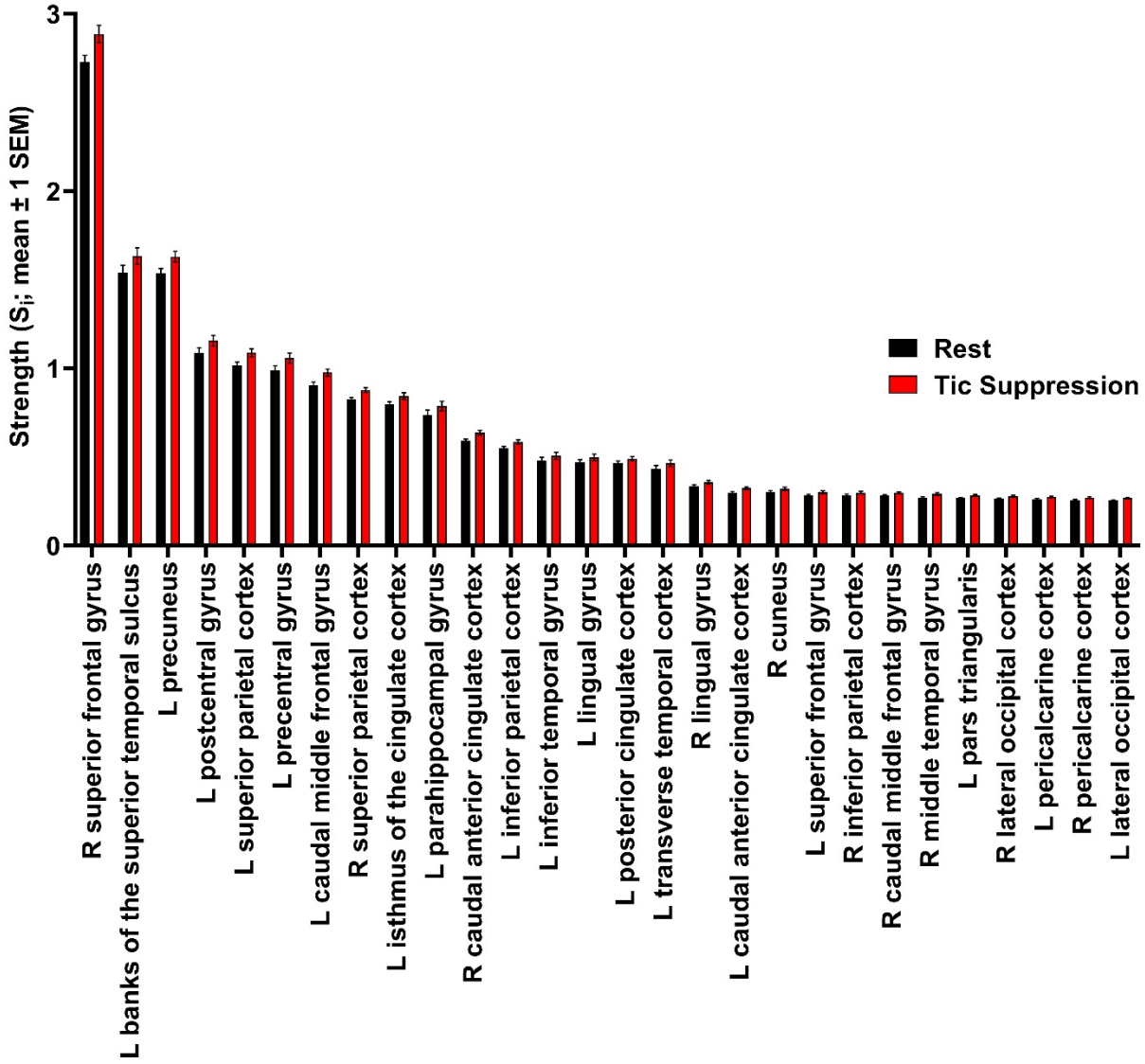

Figure S4: Connectivity strength of the nodes in the NBS subnetwork. Graph theoretical measures computed on the NBS subnetwork revealed larger strength for all nodes, at a Bonferroni-corrected threshold of α = .05 / 25 = .002. Nodes are ordered from the largest to the smallest strength value in the tic suppression condition.

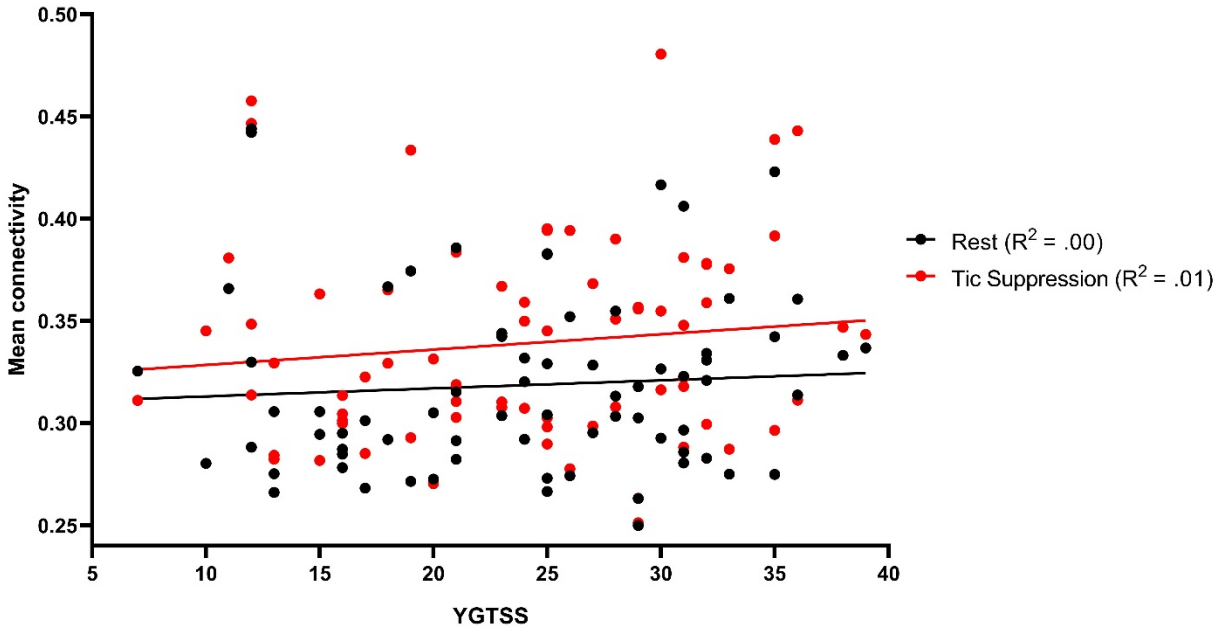

Figure S5: Mean connectivity in each condition by YGTSS scores. Within the alpha subnetwork identified by NBS, there was no interaction between condition and YGTSS scores.

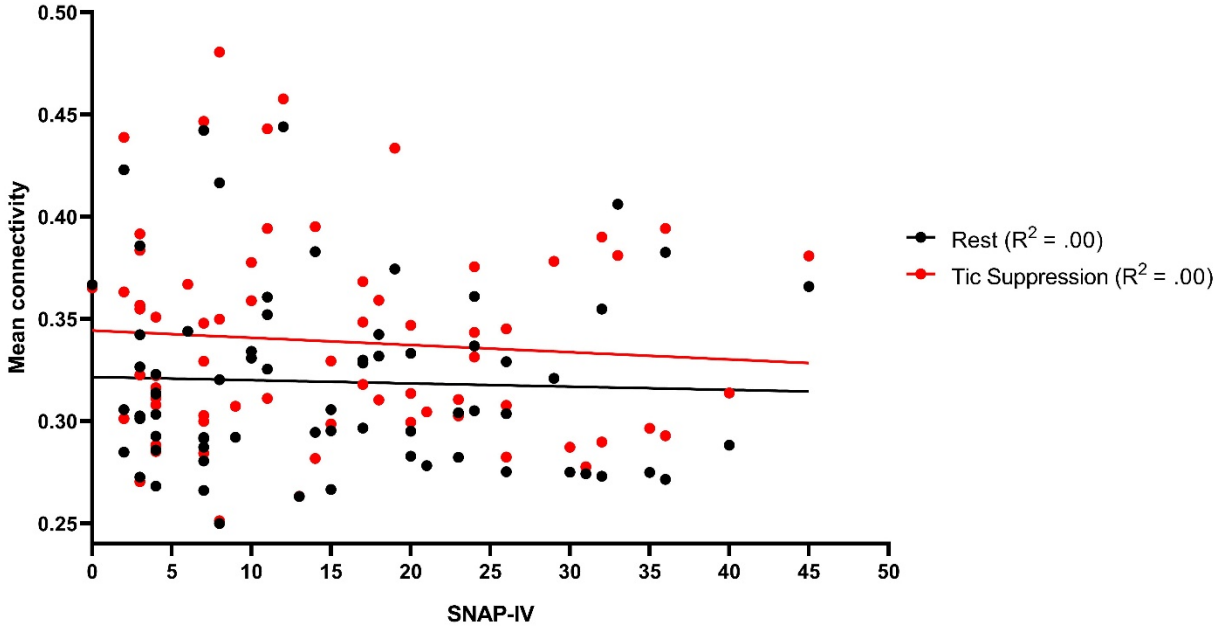

Figure S6: Mean connectivity in each condition by SNAP-IV scores. Within the alpha subnetwork identified by NBS, there was no interaction between condition and SNAP-IV scores.

Number of epochs

We tested whether there was a between-condition difference in the number of epochs that were included in our analyses. The number of valid 2-seconds epochs did not differ between tic suppression (mean = 127.4) and rest (mean = 124.4) conditions [$t(71) = 0.42$, $p = .68$, $d = .06$].

Control of methodological confounds

To ascertain that our results are not attributable to differences in the number of tic suppression sessions or duration of the rest session, we re-ran graph theory analyses pertaining to the NBS subnetwork on children with three 2-minute tic suppression sessions and 7 minutes of rest (n = 50). This did not change our results, as the within-group differences for strength [$t(49) = -.6.25$, $p < .001$, $d = .46$], characteristic path length [$t(49) = 5.84$, $p < .001$, $d = .50$], and global efficiency [$t(49) = -5.73$, $p < .001$, $d = .47$] remained significant. This suggests that increased connectivity within the NBS subnetwork during tic suppression is not attributable to variations in the number of two-minute tic suppression and the duration of rest sessions.

We also assessed whether the number of epochs had an impact on our results. We performed a repeated-measures ANCOVA on mean connectivity in the alpha-subnetwork identified through NBS, with the condition (tic suppression/rest) as a within-subjects variable and the number of epochs in the tic suppression condition, the number of epochs in the rest condition, as well as their interaction as covariates. In that analysis, neither the number of epochs in either condition nor the interaction between both variables interacted with the condition effect [all F's < 1, all p-values > .33].

Supplementary References

1. Leckman JF, Riddle MA, Hardin MT, Ort SI, Swartz KL, Stevenson J, et al. (1989): The Yale Global Tic Severity Scale: initial testing of a clinician-rated scale of tic severity. *J Am Acad Child Adolesc Psychiatry*. 28:566-573.
2. Swanson JM, Kraemer HC, Hinshaw SP, Arnold LE, Conners CK, Abikoff HB, et al. (2001): Clinical relevance of the primary findings of the MTA: success rates based on severity of ADHD and ODD symptoms at the end of treatment. *J Am Acad Child Adolesc Psychiatry*. 40:168-179.
3. Birmaher B, Brent DA, Chiappetta L, Bridge J, Monga S, Baugher M (1999): Psychometric properties of the Screen for Child Anxiety Related Emotional Disorders (SCARED): a replication study. *J Am Acad Child Adolesc Psychiatry*. 38:1230-1236.
4. Barkley RA (1997): *Defiant children: A clinician's manual for assessment and parent training, 2nd ed*. New York, NY, US: Guilford Press.
5. American Psychiatric Association (2000): *Diagnostic and statistic manual of mental disorders*. Washington, DC: Author.
6. Achenbach TM, Rescorla L (2001): *Manual for the ASEBA School-Age Forms & Profiles*. Burlington, VT: University of Vermont, Research Center for Children, Youth, and Families.
7. Wechsler D (2011): *WASI-II: Wechsler abbreviated scale of intelligence*. PsychCorp.
8. Oldfield RC (1971): The assessment and analysis of handedness: The Edinburgh inventory. *Neuropsychologia*. 9:97-113.
9. Nolan H, Whelan R, Reilly RB (2010): FASTER: Fully Automated Statistical Thresholding for EEG artifact Rejection. *J Neurosci Methods*. 192:152-162.
10. Mognon A, Jovicich J, Bruzzone L, Buiatti M (2011): ADJUST: An automatic EEG artifact detector based on the joint use of spatial and temporal features. *Psychophysiology*. 48:229-240.
11. Leach SC, Morales S, Bowers ME, Buzzell GA, Debnath R, Beall D, et al. (2020): Adjusting ADJUST: Optimizing the ADJUST algorithm for pediatric data using geodesic nets. *Psychophysiology*. n/a:e13566.
12. Tadel F, Baillet S, Mosher JC, Pantazis D, Leahy RM (2011): Brainstorm: A User-Friendly Application for MEG/EEG Analysis. *Computational intelligence and neuroscience*. 2011:879716.
13. Gramfort A, Papadopoulo T, Olivi E, Clerc M (2010): OpenMEEG: opensource software for quasistatic bioelectromagnetics. *Biomed Eng Online*. 9:45.
14. Brauchli C, Leipold S, Jäncke L (2020): Diminished large-scale functional brain networks in absolute pitch during the perception of naturalistic music and audiobooks. *NeuroImage*. 216:116513.
15. Xu T, Cullen KR, Mueller B, Schreiner MW, Lim KO, Schulz SC, et al. (2016): Network analysis of functional brain connectivity in borderline personality disorder using resting-state fMRI. *NeuroImage: Clinical*. 11:302-315.
16. Bai F, Shu N, Yuan Y, Shi Y, Yu H, Wu D, et al. (2012): Topologically convergent and divergent structural connectivity patterns between patients with remitted geriatric depression and amnestic mild cognitive impairment. *J Neurosci*. 32:4307-4318.
17. Xue K, Luo C, Zhang D, Yang T, Li J, Gong D, et al. (2014): Diffusion tensor tractography reveals disrupted structural connectivity in childhood absence epilepsy. *Epilepsy research*. 108:125-138.
18. Latora V, Marchiori M (2001): Efficient behavior of small-world networks. *Physical review letters*. 87:198701.
19. Rubinov M, Sporns O (2010): Complex network measures of brain connectivity: Uses and interpretations. *NeuroImage*. 52:1059-1069.
20. Bassett DS, Bullmore E (2006): Small-World Brain Networks. *The Neuroscientist*. 12:512-523.
21. Bassett DS, Bullmore ET (2017): Small-World Brain Networks Revisited. *The Neuroscientist : a review journal bringing neurobiology, neurology and psychiatry*. 23:499-516.
22. Watts DJ, Strogatz SH (1998): Collective dynamics of 'small-world' networks. *Nature*. 393:440-442.
23. Jia H (2019): Connectivity Analysis. In: Hu L, Zhang Z, editors. *EEG Signal Processing and Feature Extraction*. Singapore: Springer Singapore, pp 241-266.
24. Zalesky A, Fornito A, Bullmore ET (2010): Network-based statistic: Identifying differences in brain networks. *NeuroImage*. 53:1197-1207.